Histotripsy for Non-Invasive Ablation of Hepatocellular Carcinoma (HCC) Tumor in a Subcutaneous Xenograft Murine Model*

Tejaswi Worlikar[1], Eli Vlaisavljevich[2], Tyler Gerhardson[1], Joan Greve[1], Shanshan Wan[3], Sibu Kuruvilla[4], Jonathan Lundt[1], Kimberly Ives[1], Timothy Hall[1], Theodore H. Welling[3], Fred Lee[5], Zhen Xu[1]

[1]University of Michigan, Ann Arbor, MI 48109
[2]Virginia Tech University, Blacksburg, VA 24061
[3]NYU Langone Health, New York, NY 10016
[4]Stanford University, Stanford, CA 94305
[5]University of Wisconsin, Madison, WI 53792

Abstract*— Histotripsy fractionates tissue through a mechanical, non-invasive ultrasonic ablation process that precisely controls acoustic cavitation while utilizing real-time ultrasound (US) imaging guidance. This study investigates the potential, feasibility and tumor volume reduction effects of histotripsy for liver cancer ablation in a subcutaneous *in vivo* murine Hepatocellular Carcinoma (HCC) model. Hep3B tumors were generated in the right flanks of 14 NSG and 7 NOD-SCID mice. The mice were grouped as follows: A (acute, NSG with n=9 treatment and n=1 control), B (chronic, NSG with n=2 treatment and n=2 control) and C (chronic NOD-SCID, with n=6 treatment and n=1 control). Treatment was performed when the tumor diameters reached >5 mm. 1-2 cycle histotripsy pulses at 100 Hz PRF (p- >30 MPa) were delivered using a custom built 1 MHz therapy transducer attached to a motorized positioner, which scanned the transducer focus to traverse the targeted tumor volume, guided by real-time US imaging. Tumor ablation effectiveness was assessed by obtaining T1, T2 and T2* weighted MR images. Post euthanasia, treated tumor, brain, and lung tissue samples were harvested for histology. Histology of acute group A showed fractionation of targeted region with a sharp boundary separating it from untreated tissue. Groups B and C demonstrated effective tumor volume reduction post treatment on MRI as the homogenate and edema were resorbed within 2-3 weeks. However, as the tumor was subcutaneous, it was not possible to set adequate treatment margin and since the mice were immune-compromised, residual viable tumor cells eventually developed into tumor regrowth at 3-9 weeks after histotripsy. Groups B and C showed no signs of metastasis in the lung and brain. Our study successfully demonstrated the potential of histotripsy for non-invasive HCC ablation in a subcutaneous murine model. Additional work is ongoing to study the response of histotripsy in immune-competent orthotopic liver tumor models.

*Research supported by American Cancer Society.

Tejaswi Worlikar is with University of Michigan, Ann Arbor, MI 48109 USA (phone: 832-492-3002; e-mail: wtejaswi@umich.edu).

Eli Vlaisavljevich was with University of Michigan, Ann Arbor, MI 48109 USA. He is now with Virginia Tech, Blacksburg, VA 24061 USA.

Shanshan Wan and Theodore Welling were with University of Michigan, Ann Arbor, MI 48109 USA. They are now with NYU Langone Health, New York, NY 10016 USA.

Sibu Kuruvilla was with University of Michigan, Ann Arbor, MI 48109 USA. He is now with Stanford University, Stanford, CA 94305 USA.

I. Introduction

Hepatocellular Carcinoma (HCC) has been the fastest growing cancer in the United States over the past decade [1, 2]. Current treatment modalities include surgical resection, radiation, chemotherapy, and liver ablation [3, 4]. Existing liver ablation methods including radiofrequency ablation (RFA) and high intensity focused ultrasound (HIFU) [5-10] are primarily thermal-based and possess inherent limitations such as inconsistent ablation, inability to treat larger or multi-nodular tumors, limited or no real-time imaging feedback [6, 11-18] and heat sink effect through the densely vascular liver [12, 14-16]. Despite the availability of multiple treatment options, the incidence of HCC in the US has more than tripled since 1980, and the five-year survival rate is only 17% [19].

Histotripsy is the first non-invasive, non-ionizing, non-thermal ablation method that fractionates tissue through the precise control of acoustic cavitation [20-22]. Histotripsy employs focused, microsecond-length, high-amplitude ultrasound pulses to generate microbubbles from the endogenous nuclei in the target tissue [20, 22, 23]. The rapid expansion and collapse of the bubble cloud produces high strains and disrupts the surrounding cells into a liquid acellular homogenate [22, 24]. The long cooling time between ultrasound pulses (milliseconds to seconds) prevents undesirable thermal effects. Thus, histotripsy is not impeded by the heat sink effect and may safely achieve homogeneous cell disruption even in vascular organs such as liver [25]. Large vessels remain intact since they possess higher mechanical strength [26, 27] and resistance to fractionation compared to surrounding soft tissue [28, 29]. Previous studies by our group have shown that histotripsy can completely fractionate liver tissue *in vivo* in porcine and rodent models [25, 30]. In this study, our primary objective was to assess the *in vivo* ablation potential of histotripsy therapy for non-invasive treatment of subcutaneous HCC tumor in an *in vivo* murine model. We evaluated the acute and chronic response of subcutaneous xenograft HCC tumors to histotripsy therapy with the use of non-invasive Magnetic Resonance Imaging (MRI) technology and histological analysis.

978-1-5386-3646-6/18/$31.00 ©2018 IEEE

II. PROCEDURES

A. Cell Preparation

Hep3B (ATCC® HB-8064™) cells were cultivated in MEM (+Glutamine, +Earle's Salts) media supplemented with 10% FBS, 1% Antimycotic-Antibiotic, 1% Minimum non-essential amino acids (MNEAA), 1% Sodium pyruvate and 1 mL Gentamicin. The cells were maintained at 37°C in a 5% CO_2/95% humidified air atmosphere.

B. Animal Preparation

14 NSG and 7 NOD-SCID mice weighing 20-30 gm were used in this experiment. The mice were categorized into three groups: A (acute, NSG with n=9 treatment and n=1 control), B (chronic, NSG with n=2 treatment and n=2 control) and C (chronic NOD-SCID, with n=6 treatment and n=1 control). The mice were subcutaneously injected with 1-2 million Hep3B cells into the right flanks to generate xenograft tumors. The mice were monitored weekly and tumor diameter measurements were obtained using calipers. Once tumor diameters reached 5-10mm, the mice in the treatment cohorts were treated with histotripsy. This tumor treatment time-point was observed earlier in the NSG groups A and B (3-5 weeks post inoculation) as compared to the NOD-SCID group C (8-15 weeks post inoculation), which is expected based on the differences in their immunological makeup.

Prior to histotripsy, the mice were induced and maintained on general anesthesia by inhalation of isoflurane gas (1.5-2.0%) in 1 L/min of oxygen (SurgiVet V704001, Smiths Medical, Waukesha, Wisconsin, USA). The skin surrounding the subcutaneous tumor was shaved and treated with a depilatory cream. All animals were injected with Carprofen (Rimadyl, Pfizer, NY, USA) analgesic (5 mg/kg) subcutaneously prior to histotripsy therapy and once every 24 hours for 2 days after histotripsy therapy. The tumors were monitored for a week following treatment and then twice weekly for the duration of the experiment. All procedures were approved by the Committee on Use and Care of Animals at the University of Michigan.

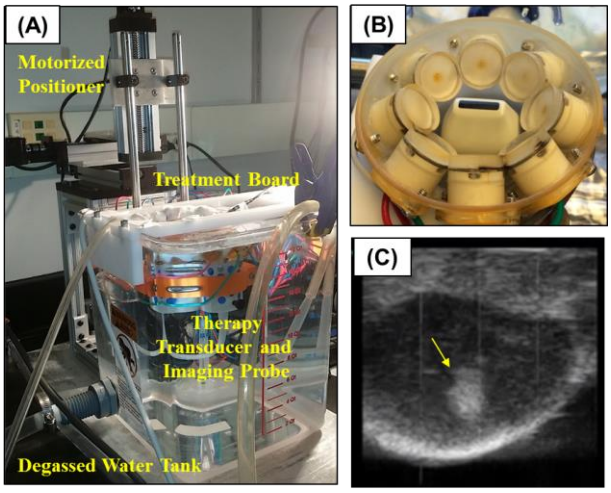

Figure 1. Experiment setup for therapy and imaging transducer mounted on the motorized positioning system and submerged in a tank of degassed water. (A) The animal is placed on the treatment board (B) 1 MHz therapeutic transducer with imaging probe coaxially mounted (C) Generation of echogenic bubble cloud in the target volume

C. Experiment Setup

A 1 MHz custom-built 8 element focused transducer designed for rodent experiments was used to generate histotripsy pulses, driven by a custom high-voltage pulser developed in-house. A field-programmable gate array (FPGA) development board (DE0-Nano Terasic Technology, HsinChu, Taiwan) specifically programmed for histotripsy therapy pulsing was connected to the pulser, allowing the therapy transducer to output 1-2 cycle histotripsy pulses. A 20 MHz probe (L40-8/12, Ultrasonix, Vancouver, Canada) was coaxially positioned with the therapy transducer for real time targeting feedback. The transducer and imaging probe were submerged in a tank of degassed water while mounted to a motorized 3-axis positioning system (Fig. 1A, Fig. 1B). A coil heater was placed into the water tank for continuous maintenance of the water temperature at 35–37°C.

C. Histotripsy Treatment

Prior to applying histotripsy, the focal position of the therapy transducer in the imaging field of view was determined by delivering test pulses to generate a bubble cloud in degassed water and marking the location of the hyperechoic region on the ultrasound imaging screen to indicate the transducer focal position in free field.

Ultrasound coupling to the targeted tumor was achieved by positioning the mice on the custom-built animal platform placed over the water tank (Fig. 1A). Tumor boundaries were manually marked on the imaging screen and input to a custom MATLAB script which generated a treatment ellipsoid with uniformly spaced treatment locations (between 0.5 mm – 0.75 mm along 3 orthogonal axes) to envelop the defined target volume. 50 histotripsy pulses at 100 Hz PRF (p- >30 MPa) were delivered each location by scanning the transducer focus using the motor positioning system. Group A was sacrificed within 3 days post treatment. Groups B and C were monitored weekly after treatment using caliper measurements and MRI for 3 months or until tumors reached ~1.8 cm.

C. Magnetic Resonance Imaging

Tumor ablation was assessed by obtaining MRI prior to histotripsy and after histotripsy, followed by weekly imaging. MRI was performed at 7.0 T using a Direct Drive console (Agilent Technologies, Santa Clara, CA, USA) with a 40 mm inner-diameter transmit-receive radiofrequency (RF) volume coil (Morris Instruments, Ontario, Canada). After pilot scans to confirm positioning, T2 and T1-weighted fast spin-echo sequences and a T2*-weighted gradient spin-echo sequence were used to visualize the tumor in the axial plane.

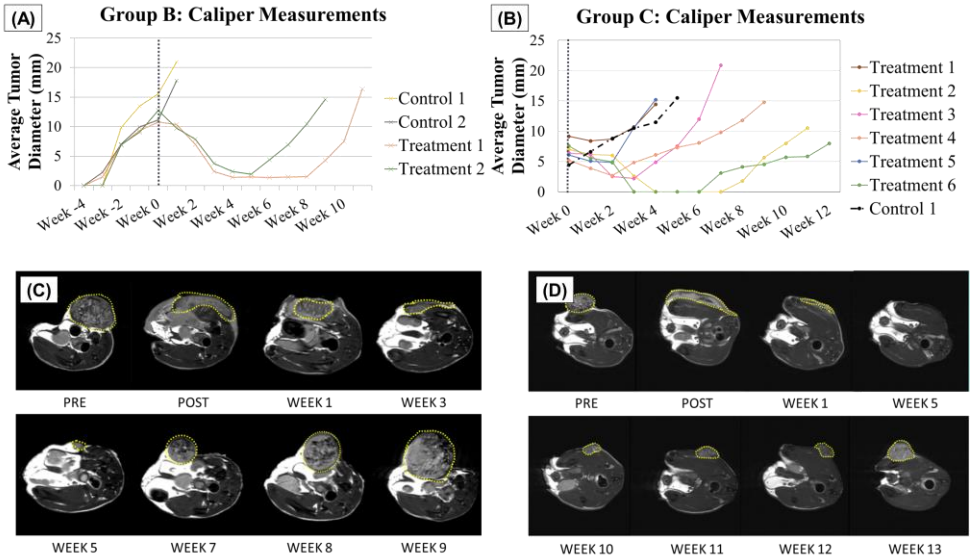

Figure 2. Tumor volume reduction effects are evidenced by caliper measurements of average treated tumor diameter following histotripsy therapy on week 0 for chronic (A) group B NSG mice and (B) group C NOD-SCID mice. Histotripsy ablation assessed using T2-weighted image in chronic (C) group B and (D) group C chronic mice respectively. The treated volume appears as homogeneous, bright area, compared to the heterogenous tumor volume with mottled signal. The yellow dashed lines show the tumor and the targeted homogenate regions

D. Histological Analysis

Post euthanasia, treated tumor, brain, and lung tissue samples were harvested for histopathology. Harvested samples were stained with hematoxylin and eosin (H&E) and examined under a microscope (Nikon Eclipse 50i).

III. RESULTS

A. Ultrasound Imaging

Histotripsy generated a bubble cloud and fractionated the targeted tumor regions guided by real-time ultrasound B-mode imaging. The bubble cloud was observed as hyperechoic (Fig. 1C) and primarily remained confined within the tumor boundaries, with transient pre-focal cavitation observed on the water-skin interface in instances when the target location point was close to the skin. Post histotripsy, the targeted region appeared as a hypoechoic zone on ultrasound imaging due to the decreased size and density of the sound scatterers.

B. Tumor Ablation Assessment

Caliper measurements demonstrated the tumor progression and post histotripsy targeted volume reduction effects in groups B and C. MRI monitoring revealed effective tumor volume reduction over time (Fig. 2A, Fig. 2B). Treated mice in group B survived longer than the control mice. MRI provided immediate as well as long term ablation feedback post histotripsy. On T2 weighted images, the targeted volume appeared homogeneous and brighter on the post-treatment image as compared to the pre-treatment image which showed a heterogeneous tumor with mottled signal (Fig. 2C, 2D). The homogenized tumor volume and edema resulting from the treatment were mostly resorbed in 2 weeks post treatment. However, any residual viable tumor cells eventually developed into tumor regrowth at 3-9 weeks after histotripsy.

B. Histological Analysis

In group A, pathology revealed fractionated tumor cells in the original sites at Day 3 post treatment (Fig. 3B). The treated region was completely fractionated into acellular debris with a sharp boundary in partially targeted tumors, though some tumor cells remained at the original site (Fig. 3C). In the chronic subset B, histology showed tumor regrowth (Fig. 3D). No metastasis was observed in the harvested distant organs in the chronic group B (Fig. 3E, Fig. 3F).

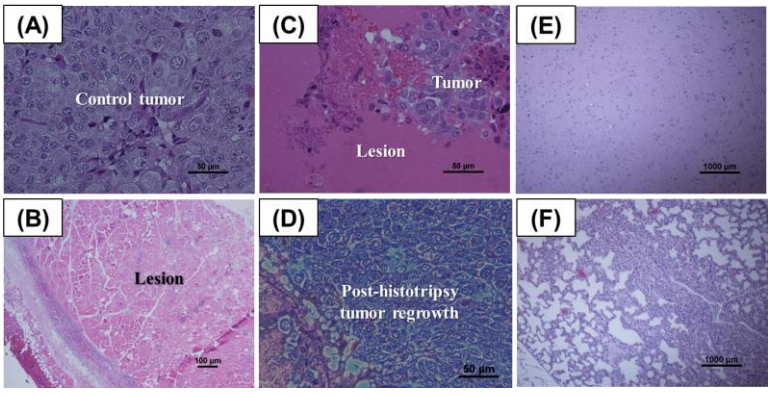

Figure 3. Histological examination revealed (A) untreated tumor in a control mouse B) absorption of homogenized tumor debris, with no tumor cells observed within or near the treatment zone at 3 days post treatment C) complete fractionation of tumor with no intact cells within the treated region in an acute mouse (D) tumors cells in post-histotripsy tumor regrowth (E) benign brain parenchyma and (F) lung parenchyma

IV. DISCUSSION

Our study investigated the effects of histotripsy tumor ablation in an acute and chronic xenograft murine model. Histotripsy generated well-confined bubble clouds resulting in the formation of completely fractionated histotripsy lesions with sharply demarcated boundaries between the surrounding healthy liver tissue and the lesion. In the weeks following histotripsy treatment, a steady reduction in the volume of the treated homogenate was observed. However, as this subcutaneous tumor model did not allow sufficient treatment margin and the mice were

immune-compromised, any post-treatment residual viable tumor cells eventually developed into tumor regrowth at 3-9 weeks after histotripsy. In instances where we attempted to define a margin outside the tumor region, post-treatment and weekly follow-up MRI revealed surrounding leg muscle damage and edema near the treatment region. However, this healed completely within 1-2 weeks and no further evidence of damage was observed. The immunocompromised nature of the murine hosts did not allow us to examine the role of the immune system in tumor progression in this model. Future work is ongoing to investigate the long-term effects of histotripsy liver cancer ablation in immunocompetent orthotopic rodent liver tumor model.

MRI successfully enabled immediate assessment of post histotripsy ablation of tumor which may be a significant clinical benefit for histotripsy over other thermal ablation therapies, in which the treatment effectiveness can only be assessed after a few weeks of therapy [15, 31]. Future work is ongoing to quantitatively characterize the MRI observations and investigate the use of alternative imaging sequences or contrast agents in order to optimally distinguish healthy tissue, residual tumor tissue, and the fractionated histotripsy tissue homogenate on post histotripsy scans. This will be useful in planning follow-up histotripsy treatments to target any detected residual tumor and improve survival rates by preventing recurrence.

V. Conclusion

This study demonstrates the potential of histotripsy for non-invasive HCC ablation and subsequent tumor volume reduction in a subcutaneous murine model. Further work is ongoing to study the biological response of histotripsy in immune-competent orthotopic liver tumor rodent models.

References

[1] F. X. Bosch, J. Ribes, M. Diaz, and R. Cleries, "Primary liver cancer: worldwide incidence and trends," (in eng), *Gastroenterology,* vol. 127, no. 5 Suppl 1, pp. S5-S16, Nov 2004.

[2] H. B. El-Serag and A. C. Mason, "Rising incidence of hepatocellular carcinoma in the United States," (in eng), *N Engl J Med,* vol. 340, no. 10, pp. 745-50, Mar 11 1999.

[3] T. Livraghi, H. Makisalo, and P. D. Line, "Treatment options in hepatocellular carcinoma today," (in eng), *Scand J Surg,* vol. 100, no. 1, pp. 22-9, 2011.

[4] L. Rossi *et al.*, "Current approach in the treatment of hepatocellular carcinoma," (in eng), *World J Gastrointest Oncol,* vol. 2, no. 9, pp. 348-59, Sep 2010.

[5] R. M. Charnley, J. Doran, and D. L. Morris, "Cryotherapy for liver metastases: a new approach," (in eng), *Br J Surg,* vol. 76, no. 10, pp. 1040-1, Oct 1989.

[6] C. Erce and R. W. Parks, "Interstitial ablative techniques for hepatic tumours," (in eng), *Br J Surg,* vol. 90, no. 3, pp. 272-89, Mar 2003.

[7] H. W. Head and G. D. Dodd, 3rd, "Thermal ablation for hepatocellular carcinoma," (in eng), *Gastroenterology,* vol. 127, no. 5 Suppl 1, pp. S167-78, Nov 2004.

[8] T. A. Leslie and J. E. Kennedy, "High-intensity focused ultrasound principles, current uses, and potential for the future," (in eng), *Ultrasound Q,* vol. 22, no. 4, pp. 263-72, Dec 2006.

[9] E. Liapi and J. F. Geschwind, "Transcatheter and ablative therapeutic approaches for solid malignancies," (in eng), *J Clin Oncol,* vol. 25, no. 8, pp. 978-86, Mar 10 2007.

[10] G. ter Haar, "High intensity ultrasound," (in eng), *Semin Laparosc Surg,* vol. 8, no. 1, pp. 77-89, Mar 2001.

[11] A. J. Aschoff *et al.*, "How does alteration of hepatic blood flow affect liver perfusion and radiofrequency-induced thermal lesion size in rabbit liver?," (in eng), *J Magn Reson Imaging,* vol. 13, no. 1, pp. 57-63, Jan 2001.

[12] S. A. Curley, "Radiofrequency ablation of malignant liver tumors," (in eng), *Oncologist,* vol. 6, no. 1, pp. 14-23, 2001.

[13] M. Kudo, "Radiofrequency ablation for hepatocellular carcinoma: updated review in 2010," (in eng), *Oncology,* vol. 78 Suppl 1, pp. 113-24, Jul 2010.

[14] D. S. Lu *et al.*, "Influence of large peritumoral vessels on outcome of radiofrequency ablation of liver tumors," (in eng), *J Vasc Interv Radiol,* vol. 14, no. 10, pp. 1267-74, Oct 2003.

[15] J. A. Marrero and S. Pelletier, "Hepatocellular carcinoma," (in eng), *Clin Liver Dis,* vol. 10, no. 2, pp. 339-51, ix, May 2006.

[16] E. J. Patterson, C. H. Scudamore, D. A. Owen, A. G. Nagy, and A. K. Buczkowski, "Radiofrequency ablation of porcine liver in vivo: effects of blood flow and treatment time on lesion size," (in eng), *Ann Surg,* vol. 227, no. 4, pp. 559-65, Apr 1998.

[17] T. A. Leslie *et al.*, "High-intensity focused ultrasound ablation of liver tumours: can radiological assessment predict the histological response?," (in eng), *Br J Radiol,* vol. 81, no. 967, pp. 564-71, Jul 2008.

[18] A. Okada *et al.*, "A case of hepatocellular carcinoma treated by MR-guided focused ultrasound ablation with respiratory gating," (in eng), *Magn Reson Med Sci,* vol. 5, no. 3, pp. 167-71, Oct 2006.

[19] T. Loftsson, D. Hreinsdottir, and M. Masson, "Evaluation of cyclodextrin solubilization of drugs," *International Journal of Pharmaceutics,* vol. 302, no. 1-2, pp. 18-28, 2005.

[20] J. E. Parsons, C. A. Cain, G. D. Abrams, and J. B. Fowlkes, "Pulsed cavitational ultrasound therapy for controlled tissue homogenization," (in eng), *Ultrasound Med Biol,* vol. 32, no. 1, pp. 115-29, Jan 2006.

[21] W. W. Roberts, T. L. Hall, K. Ives, J. S. Wolf, Jr., J. B. Fowlkes, and C. A. Cain, "Pulsed cavitational ultrasound: a noninvasive technology for controlled tissue ablation (histotripsy) in the rabbit kidney," (in eng), *J Urol,* vol. 175, no. 2, pp. 734-8, Feb 2006.

[22] Z. Xu *et al.*, "Controlled ultrasound tissue erosion," (in eng), *IEEE Trans Ultrason Ferroelectr Freq Control,* vol. 51, no. 6, pp. 726-36, Jun 2004.

[23] A. D. Maxwell, C. A. Cain, T. L. Hall, J. B. Fowlkes, and Z. Xu, "Probability of cavitation for single ultrasound pulses applied to tissues and tissue-mimicking materials," (in eng), *Ultrasound Med Biol,* vol. 39, no. 3, pp. 449-65, Mar 2013.

[24] A. D. Maxwell *et al.*, "Cavitation clouds created by shock scattering from bubbles during histotripsy," (in eng), *J Acoust Soc Am,* vol. 130, no. 4, pp. 1888-98, Oct 2011.

[25] E. Vlaisavljevich *et al.*, "Non-Invasive Ultrasound Liver Ablation Using Histotripsy: Chronic Study in an In Vivo Rodent Model," (in eng), *Ultrasound Med Biol,* vol. 42, no. 8, pp. 1890-902, Aug 2016.

[26] G. Zhao *et al.*, "Mechanical stiffness of liver tissues in relation to integrin beta1 expression may influence the development of hepatic cirrhosis and hepatocellular carcinoma," *J Surg Oncol.,* Research Support, Non-U.S. Gov't vol. 102, no. 5, pp. 482-9., Oct 1 2010.

[27] Umale S *et al.*, "Experimental in vitro mechanical characterization of porcine Glisson's capsule and hepatic veins," *J Biomech,* vol. 44, no. 9, pp. 1678-83, 2011.

[28] E. Vlaisavljevich, Y. Kim, G. Owens, W. Roberts, C. Cain, and Z. Xu, "Effects of tissue mechanical properties on susceptibility to histotripsy-induced tissue damage," (in eng), *Physics in Medicine and Biology,* vol. 59, no. 2, pp. 253-70, Jan 20 2014.

[29] E. Vlaisavljevich, A. Maxwell, M. Warnez, E. Johnsen, C. Cain, and Z. Xu, "Histotripsy-induced cavitation cloud initiation thresholds in tissues of different mechanical properties," (in eng), *IEEE Transactions on Ultrasonics, Ferroelectrics, and Frequency Control,* vol. 61, no. 2, pp. 341-52, Feb 2014.

[30] E. Vlaisavljevich *et al.*, "Image-guided non-invasive ultrasound liver ablation using histotripsy: feasibility study in an in vivo porcine model," (in eng), *Ultrasound Med Biol,* vol. 39, no. 8, pp. 1398-409, Aug 2013.

[31] J. E. Coad, K. Kosari, A. Humar, and T. D. Sielaff, "Radiofrequency ablation causes 'thermal fixation' of hepatocellular carcinoma: a post-liver transplant histopathologic study," (in eng), *Clin Transplant,* vol. 17, no. 4, pp. 377-84, Aug 2003.